Chains of Cobalt Doped Magnetosomes Extracted from AMB-1 Magnetotactic Bacteria for Application in AMF hyperthermia

E. Alphandery, C. Carvallo, N. Menguy, I. Chebbi

Chains of Cobalt doped magnetosomes synthesized by AMB-1 magnetotactic bacteria for application in AMF hyperthermia

E. Alphandéry[+], C. Carvallo[+], N. Menguy[+], I. Chebbi[*].

[+] Université Pierre et Marie-Curie, Institut de Minéralogie et de physique de la matière condensée (IMPMC), 140 rue de Lourmel, 75015 Paris, France.

*Nanobacterie SARL, 36 boulevard Flandrin, 75016 Paris, France.

Abstract:

We demonstrate how to improve the heating properties of chains of magnetosomes synthesized by AMB-1 magnetotactic bacteria, which can be used for alternative magnetic field (AMF) hyperthermia. This is achieved by introducing cobalt quinate within the bacterial growth medium, resulting in Cobalt doped magnetosomes.

New treatments of cancer use nanoparticles as therapeutic agents. Among the different approaches tested, it has been suggested to send iron oxide nanoparticles within cancer cells and then kill these cells by heating them under the application of an alternative magnetic field (AMF). This technique has been tested on animals by several different groups (1-3) and is now at the stage of clinical trials for several different cancers, such as prostate, esophageal and pancreatic cancers (4). This technology can be improved further by increasing the specific absorption rate (SAR) of the nanoparticles currently tested. One way to achieve this aim is to dope the iron oxide nanoparticles with cobalt (5-16). Indeed, the insertion of cobalt within the iron oxide nanoparticles results in increasing hysteresis losses and nanoparticle SAR (17). Although encouraging, this property has been obtained for a rather large percentage of cobalt doping. An increase by a factor of two of the magnetocrystalline anisotropy constant is reached for a percentage of Co-doping larger than 10 % (18), (19). For such a large percentage of cobalt doping, the medical applications of these chemically synthesized iron oxide nanoparticles are uncertain due to the risks of toxicity.

In order to lower the percentage of cobalt doping while still retaining the desired magnetic properties, cobalt doped iron oxide nanoparticles can be synthesized biologically by using magnetotactic bacteria (20). Indeed, when they are grown in the presence of cobalt quinate, AMB-1 magnetotactic bacteria synthesize iron oxide nanoparticles, called magnetosomes, which contain a percentage of cobalt lying between 0.2 and 1.4 % (20). It has been shown that the magnetic properties of these cobalt doped magnetosomes are considerably improved even for such a low percentage of cobalt doping (20).

In this letter, we provide an explanation for the change of the magnetic properties of cobalt doped magnetosomes. We show that this behavior is essentially due to two factors, i. e. the increase of the magnetosome interactions in the presence of cobalt and the arrangement of the magnetosomes in chains (21). We also demonstrate that chains of magnetosomes extracted from magnetotactic bacteria, which

are currently tested for cancer thermotherapy (22), produce a larger SAR when they are doped with cobalt than when they are undoped.

Magnetospirillum magneticum strain AMB-1 was purchased from the ATCC (ATCC 700274). Cells were grown microanaerobically at room temperature (~25°C) in liquid culture in MSGM medium (ATCC Medium 1653). Undoped magnetosomes were obtained by introducing only iron ions (Fe^{2+} or Fe^{3+}) in the growth medium using an iron quinate solution (21, 23). Co-doped magnetosomes were synthesized by introducing a 20 μM cobalt quinate solution in addition to the iron source. Different types of samples were then prepared, containing either whole magnetotactic bacteria, chains of magnetosomes extracted from magnetotactic bacteria and individual magnetosomes unbound from the chains, which were obtained by heat and SDS treatments of the extracted chains of magnetosomes. Details about the sample preparations are given in the supplementary information section.

Two electron microscopes were used to characterize the magnetosomes. A JEOL (100 kV) model JEM 1011 transmission electron micrograph (TEM) was used to obtain low-magnification micrographs of the different samples mentioned above. For that, 10 μl of suspensions containing either whole bacteria, extracted chains of magnetosomes, or individual magnetosomes with $2\ 10^{-4}$ % by weight of magnetosomes were deposited on top of a carbon grid. After it had dried, the carbon grids containing the different suspensions were placed inside the electron microscope for analysis. A JEOL 2100F was used to carry out energy electron loss spectroscopy (EELS) on single magnetosomes and to verify that the magnetosomes synthesized in the presence of cobalt quinate contained cobalt. As shown in the supplementary information section, the EELS spectrum of the magnetosomes synthesized in the presence of cobalt quinate (Suppl. Fig. 1(b)) shows a peak arising from cobalt. This confirms the presence of cobalt within the magnetosomes synthesized in these conditions (20).

To characterize the magnetic properties of the different samples, a vibrating sample magnetometer (VSM) from Quantum Design and an alternative gradient magnetometer (AGM) from Princeton Measurements Corporation were used. For that, 25 µl of suspensions of whole bacteria, extracted chains of magnetosomes, or individual magnetosomes containing 4 10^{-4} % by weight of magnetosomes were deposited on top of a silica substrate (50 x 50 mm^2). After it had dried, the silica substrates covered by the different suspensions were placed inside a VSM or AGM for magnetic measurements. We measured hysteresis loops of the different samples at 20 K and 300 K using a VSM and room temperature First Order Reversal Curve (FORC) diagrams using an AGM. Details about the principles of the FORC diagrams can be found in the supplementary information section. From the FORC diagrams, we deduced the distributions of mean interacting field, H_u, of the local interacting field, ΔH_u, and of the microcoercivity, H_c, which is similar to the coercivity estimated by hysteresis loop measurements except that in this case the samples are subjected to a series of magnetic fields of different strengths.

The focus of this letter is the study of chains of magnetosomes extracted from the bacteria, which have been shown to be efficient for cancer thermotherapy (22). Fig. 1(a) shows a TEM micrograph of typical chains of magnetosomes extracted from magnetotactic bacteria. This sample is characterized by the presence of chains of magnetosomes containing more than 10 magnetosomes in average. To characterize the magnetic properties of these chains, hysteresis loops of the extracted chains of magnetosomes were measured at 20 K. Figure 1(b) shows that between the undoped and Co-doped magnetosomes, the coercivity increases from $H_c \sim 360$ Oe up to $H_c \sim 3130$ Oe. Assuming that for such a low level of Co-doping (< 2 %, (20)), the saturation magnetization of the assembly of magnetosomes is that of maghemite and using the relation $K_{eff} \sim M_s H_c/2$, where K_{eff} reflects the average magnetocrystalline anisotropy constant associated to each magnetosome, we estimate that K_{eff} increases from $K_{eff} \sim 12$ KJ/m^3 in the absence of cobalt up to $K_{eff} \sim 104$ KJ/m^3 in the presence of cobalt.

To understand if the origin of this behavior is due to increasing interactions between the magnetosomes in the presence of cobalt, we have carried out FORC measurements at 300 K. These measurements enable an estimate of the mean and local interacting fields, which reflect the strength of the interactions between the magnetosomes. The FORC diagrams of the extracted chains of magnetosomes are shown in Figs. 2 for the magnetosomes synthesized either in the absence (Fig. 2(a)) or in the presence (Fig. 2(b)) of cobalt. The FORC distribution is displaced below the H_u=0 axis, showing that the mean interacting field, H_u, is weak but non-zero and negative, indicating the presence of weak interactions between the chains of magnetosomes (23). Moreover, the mean interacting field increases in magnitude from H_u ~ - 1 mT in the absence of cobalt (Fig. 2(a)) up to H_u ~ - 2.3 mT (Fig. 2(b)) in the presence of cobalt. The local interacting field, ΔH_u, estimated from the FWHM of the distribution of interacting fields across the maximum H_c value, also increases from ~ 7 mT in the absence of cobalt up to ~ 11 mT in the presence of cobalt (Figs. 2(a) and 2(b)). These results indicate that there is an enhancement of the interactions between the magnetosomes in the presence of cobalt and that this enhancement could cause the change of the magnetic properties observed between Figs. 2(a) and 2(b).

To discern between the role played by these interactions and by the arrangement of the magnetosomes in chains, we have studied the properties of two other samples. The first one contains whole magnetotactic bacteria in which the chains of magnetosomes are well separated and non-interacting (Suppl. Fig. 2(c)). The coercivity increases by ~ 40 % in the presence of cobalt (Suppl. Figs. 2(a) and 2(b)). This increase is much smaller than that of ~ 75 % observed for the extracted chains of magnetosomes (Figs. 2(a) and 2(b)). We conclude that interaction between the chains of magnetosomes is one of the parameters, which produces the change of the magnetic of the extracted chains of magnetosomes synthesized in the presence of cobalt. To study the role played by the local interacting

field and by the alignment of the [111] crystallographic planes of the magnetosomes contained within the chains, we have studied another sample containing individual magnetosomes unbound from the chains, which don't have their [111] crystallographic planes aligned in a preferential direction (Suppl. Fig. 3, 21). In this sample, the local interacting field and coercivity remain relatively unaffected by the presence of cobalt. They remain constant at $H_c \sim 40 \pm 2$ mT and $\Delta H_u \sim 9 \pm 1$ mT between the undoped and doped sample (Suppl. Figs. 4(a) and 4(b)). From these results, we conclude that the change of the magnetic properties observed in the presence of cobalt is partly due to the increase of the mean and local interacting fields and partly to the arrangement of the magnetosomes in chains.

The heating efficiency of the co-doped magnetosomes arranged in chains and extracted from the bacteria has also been studied. For that, 100 µl of a suspension containing extracted chains of magnetosomes with ~ 1.5 mg of maghemite per milliliter is submitted to an alternative magnetic field of frequency 183 KHz and field amplitude 80 mT. As can be seen in Figure 3, the application of the alternative magnetic field produces a larger temperature increase for the co-doped magnetosomes (34 °C in 15 minutes) than for the undoped magnetosomes (27 °C in 15 minutes). We also estimated a higher SAR of ~ 500 W/g_{Fe} for the cobalt doped magnetosomes than for the undoped magnetosomes (SAR ~ 400 W/g_{Fe}), (24). This indicates an enhancement of the heating capability of the chains of magnetosomes extracted from bacteria, which have been cultivated in the presence of cobalt quinate.

In conclusion, we have shown in this letter that the change of the magnetic properties of Co-doped magnetosomes is due to their arrangement in chains. For this reason, the change of the magnetic properties induced by the presence of cobalt is observed for a percentage of cobalt within the magnetosomes, which is smaller than that usually obtained with chemically synthesized nanoparticles, which are not arranged in chains. Furthermore, we have shown that the cobalt doped magnetosomes

arranged in chains produce a larger amount of heat than the undoped magnetosomes arranged in chains when they are exposed to an alternative magnetic field.

Acknowledgment: We thank Fériel Skouri-Panet for her help with the culture of the bacteria. We thank Eric Larquet and Jean-Michel Guigner for their help with TEM measurements.

Figures:

Figure 1:

(a): A TEM micrograph of the chains of magnetosomes extracted from the whole bacteria. (b): Hysteresis loops measured at 20 K of the extracted chains of magnetosomes synthesized in the absence of cobalt quinate (blue line) or in the presence of cobalt quinate (black line).

Figure 2:

FORC diagrams measured at 300 K of the extracted chains of magnetosomes synthesized in the absence of cobalt quinate, (a), or in the presence of cobalt quinate, (b).

Figure 3:

Increase in temperature observed when a suspension of chains of magnetosomes extracted from AMB-1 magnetotactic bacteria is subjected to an alternative magnetic field of frequency 183 KHz and amplitude 80 mT.

Supplementary Figure 1:

EELS spectra of the extracted chains of magnetosomes synthesized in the absence of cobalt quinate, (a), or in the presence of cobalt quinate, (b).

Supplementary Figure 2:

FORC diagrams measured at 300 K of the whole magnetotactic bacteria synthesized in the absence of cobalt quinate, (a), or in the presence of cobalt quinate, (b). (c): A TEM micrograph of two whole magnetotactic bacteria.

Supplementary Figure 3:

TEM micrograph of the individual magnetosomes prepared by heat and SDS treatments of the extracted chains of magetosomes.

Supplementary Figure 4:

FORC diagrams measured at 300 K of the individual magnetosomes synthesized in the absence of cobalt quinate, (a), or in the presence of cobalt quinate, (b).

Supplementary information section:

Supplementary information:

Sample preparation:

Details about the growth conditions of AMB-1 magnetotactic bacteria including their growth curves can be found elsewhere (Yang. et al, *Enz. Microb. Techno.* 29, 13-19 (2001), ATCC protocol to grow strain AMB-1/700264, ATCC growth medium 1653 available on the website of the ATCC). Cells were harvested at stationary phase. Stationary phase occurred when the medium became completely reduced as indicated by a change in the coloration of the growth medium, from pink to colorless. Three different types of samples were prepared. The living bacteria were first centrifuged at 8000 rpm for 15 minutes. The solution was then placed against a magnet and the supernatant containing the growth medium was removed and replaced by 2 ml of deionized water. Hence we obtained 2 ml of a solution of whole bacteria dispersed in water, which we redispersed in a 10 mM Tris buffer and sonicated during 60 minutes at 30 W to extract the chains of magnetosomes from the whole bacteria. After sonication the solution containing the extracted chains of magnetosomes was placed against a magnet and the supernatant was removed to get rid of most of the biogenic material. The solution was washed 10 times in this way. 1 ml of this solution was transferred into an ependorf tube and was not treated further. It contained the extracted chains of magnetosomes. 1 ml of the same solution was transferred in another ependorf tube and heated for one hour at 90 ^{0}C in the presence of 1 % sodium dodecyl sulfate (SDS). The solution was heated by placing the ependorph inside boiling water. The second solution contained the individual magnetosomes, which were both extracted from the whole bacteria and detached from the chains.

Electron energy loss spectroscopy measurements:

In order to determine that the magnetosomes synthesized in the presence of cobalt quinate were doped with cobalt, electron energy loss spectroscopy measurements were carried out on a series of individual magnetosomes. For the magnetosomes produced in the absence of quinate cobalt, Suppl. Fig.

1(A) only shows two peaks at 710 eV and 720 eV, which are attributed to the L2 and L3 peaks of iron. This indicates that the magnetosomes are pure iron oxide in this case. For the magnetosomes produced in the presence of a 20 μM cobalt quinate solution, the L2 and L3 peaks of iron are still present but in addition, we observe the L2 peak of cobalt at 780 eV in the EELS spectrum (Suppl. Fig. 1(B).

First order reversal curve measurements:

FORC diagrams, which were measured at the Laboratoire des Sciences du Climat et de l'Environnement (LSCE), Gif-sur-Yvette, France, are constructed by measuring partial magnetic hysteresis curves known as first-order reversal curves or FORCs (Pike *et al*, *J. Appl. Phys.* 85, 6660-6667 (1999), Roberts et al, *J. Geophys. Res.* 105, 28,461-28,475 (2000)). Starting at positive saturation, the applied field is decreased until a specified reversal field (H_r) is reached. A FORC is the magnetization curve measured at regular field steps from H_r back up to positive saturation. A large number of FORCs is measured, so that the FORCs fill the interior of a major hysteresis loop. The magnetization (M) on the FORC with reversal field H_r is denoted by $M(H_r, H)$. The FORC distribution is defined as the mixed second derivative:

$$\rho(H_r, H) \equiv -\frac{\partial^2 M(H_r, H)}{\partial H_r \partial H},$$

which is well defined for $H > H_r$.

When plotting FORC distributions on FORC diagrams, it is customary to change coordinates from $\{H_r, H\}$ to $H_c = (H - H_r)/2$ and $H_u = (H + H_r)/2$ (Chen et al, *J. Geophys. Res.* 112, B08S90, doi:10.1029/2006JB004575 (2007). FORC diagrams provide an alternative method of measuring Preisach distributions, which gives information about the spectrum of coercivity and interaction field within a sample (26, 27). In the case of ideal single-domain (SD) grains and under the assumption that Hc and Hu are fixed for each grain but different from grain to grain, the FORC function is equivalent

to a Preisach function. According to Néel's interpretation (Néel, L.; *Appl. Sci. Res. Sect B* 4, 13-24 (1954)), the distribution along the H_c axis is equivalent in a first approximation to the distribution of particle microcoercivities, and a cross-section through the peak of the FORC distribution parallel to the H_u axis left of the central peak is equivalent to the distribution of magnetostatic interaction fields. However, the exact theory developed by Egli (Egli, *Geophys. Res.*, 111, B12S17, doi: 10.1029/2006JB004567 (2006)) shows that the accurate representation of the coercivity distribution of SD particles is the marginal distribution (Winklhofer et al; *J. Appl. Phys.* 99, 08E710, doi:10.1063/1.2176598 (2006)). Measurements of FORC diagrams on natural and synthetic samples have provided the following interpretative framework (Roberts et al; *J. Geophys. Res.* 105, 28,461-28,475 (2000), Winklhofer et al; *J. Appl. Phys.* 99, 08E710, doi:10.1063/1.2176598 (2006), Muxworthy et al; *J. Geophys. Res.* 108(B11), 2517, doi: 10.1029/2003JB002588 (2003). SD particles are characterized by closed concentric contours about a central peak, while FORC diagram of multi-domain particles go from contours that diverge away from the horizontal axis close to the origin, to nearly vertical contours with the peak close to Hc=0. Two sorts of FORC diagram features can be caused by interactions. Firstly, a shift of the FORC diagram maximum above or below the H_c=0 axis is caused by negative or positive mean interaction field, respectively (Stancu et al, *J. Appl. Phys.* 93, 6620-6622 (2003), Pike et al; *J. Appl. Phys.* 85, 6660-6667 (1999). Secondly, the spreading of the FORC contours parallel to the H_u axis indicates the presence of a local interaction field (Pike et al; *J. Appl. Phys.* 85, 6660-6667 (1999). One hundred FORCs were measured to construct each FORC diagram. The smoothing factor (Roberts et al; *J. Geophys. Res.* 105, 28,461-28,475 (2000)) was set at 3 for all the FORC diagrams.

References:

1. DeNardo, S., J.; DeNardo, G., L.; Miers, L., A.; Natarajan, A.; Foreman, A., R.; Gruettner, C.; Adamson, G., N.; Ivkov, R.; *Clin. Cancer Res.* **11**, 7087s (2005).
2. Ito, A.; Tanaka, K.; Honda, H.; Abe, S.; Yamaguchi, H.; Kobayashi, T.; *J. Bioscience Bioengineering* **96**, 364 (2003).
3. Kawai, N.; Futakuchi, M.; Yoshida, T.; Ito, A.; Sato, S.; Naiki, T.; Honda, H.; Shirai, T.; Kohri, K.; *The Prostate* **68**, 784 (2008).
4. See the website of the German company Magforce Nanotechnologies AG, www.magforce.de, for more information on clinical trials.
5. Ahmed, S., R.; Ogale, S. B.; Papaefthymiou, G. C.; Ramesh, R.; Kofinas, P.; *Appl. Phys. Lett.* **80**, 1616 (2002).
6. Bala, T.; Sankar, C. R.; Baidakova, M.; Osipov, V.; Enoki, T.; Joy, P. A.; Prasad, L., V.; Sastry, M.; *Langmuir* **21**, 10638 (2005).
7. Baldi, G.; Bonacchi, D.; Innocenti, G.; Lorenzi, G. ; Sangegorio, C. ; *J. Magn. Magn. Mat.* **311**, 10 (2007).
8. Canna, C.; Ardu, A.; Musinu, A.; Peddis, D.; Piccaluga, G.; *Chem. Mater.* 20, 6364 (2008).
9. Junor, A., F.; Zapf, V.; Egan, P.; *Journ. Appl. Phys.* **101**, 09M506-1 (2007).
10. Giri, A. K.; Kirkpatrick, E. M.; Moongkhamklang, P.; Majetich, S. A.; *Appl. Phys. Lett.* **80**, 2341 (2002).
11. Mooney, K. E.; Nelson, J. A.; Wagner M. J.; *Chem. Mater.* **16**, 3155 (2004).
12. Lee, J. G.; Park, J. Y.; Kim, C. S.; *J. Mater. Sci.* **33**, 3965 (1998).
13. Pillai, V.; Shah, D. O.; *J. Magn. Magn. Mater.* **163**, 243 (1996).
14. Seip, C. T.; Carpenter, E., E.; O'Connor, C., J.; *IEEE Trans. Magn.* **34**, 1111 (1998).
15. Uzunova, E. ; Klissurski, D.; Mitov, I.; Stefanov, P.; *Chem. Mater.* **162**, 331 (1996).

16. Yan, C., H.; Xu, Z. G.; Cheng, F. X.; Wang, Z. M.; Sun, L. D.; Liao, C. S.; Jia, J. T.; *Solid State Commun.* **111**, 287 (1999).

17. Veverka, M.; Veverka, P.; Kaman, O.; Lanëok, A.; Závèvta, K.; Pollet, E.; Knízek, K.; Báhaèek, J.; Benes, M.; Kaspar, P.; Duguet, E.; Vasseur, S.; Nanotechnology **18**, 345704 (2007).

18. Franco, A. Jr.; Zapf, V. J. Mag. Mag. Mat. **320**, 709 (2008).

19. Tackett, R.; Sudakar, C.; Naik, R.; Lawes, G.; Rablau, C.; Vaishnava, P., P; *J. Magn. Magn. Mater.*, **320**, 2755 (2008).

20. Staniland, S.; Williams, W.; Telling, N.; Van Der Laan, G., Harrison, A.; Ward, B.; *Nature Nanotechnology* **3**, 158 (2008).

21. Alphandéry, E., Ding, Y., Ngo, A.T., Wu, L.F., Pileni, M.P.; *ACS Nano* **3**, 1539 (2009).

22. We have injected a suspension of extracted chains of magnetosomes within tumor mice, which we have then heated by applying an alternative magnetic field and we have shown that this yielded anti-tumoral activity (the disappearance of the tumor 30 days after the treatment). For suspensions containing individual magnetosomes or whole bacteria injected within the tumor mice, we have not observed any anti-tumoral activity.

23. Alphandéry, E.; Ngo, A., T.; Lefevre, C.; Lisiecki, I.; Wu, L., F.; Pileni, M., P.; *J. Phys. Chem. C* **112**, 12304 (2008).

24. To measure the SAR, we use the formula $SAR = C_{water}\left(\frac{\Delta T}{\delta t}\right)\frac{1}{x_m}$, where C_{water} is the specific heat capacity of water (C_{water} = 4.184 J/g.K), x_m is the concentration of iron in g per mL of solvent (water) and ($\Delta T/\delta T$) is the variation with time of the temperature measured at 25°C.

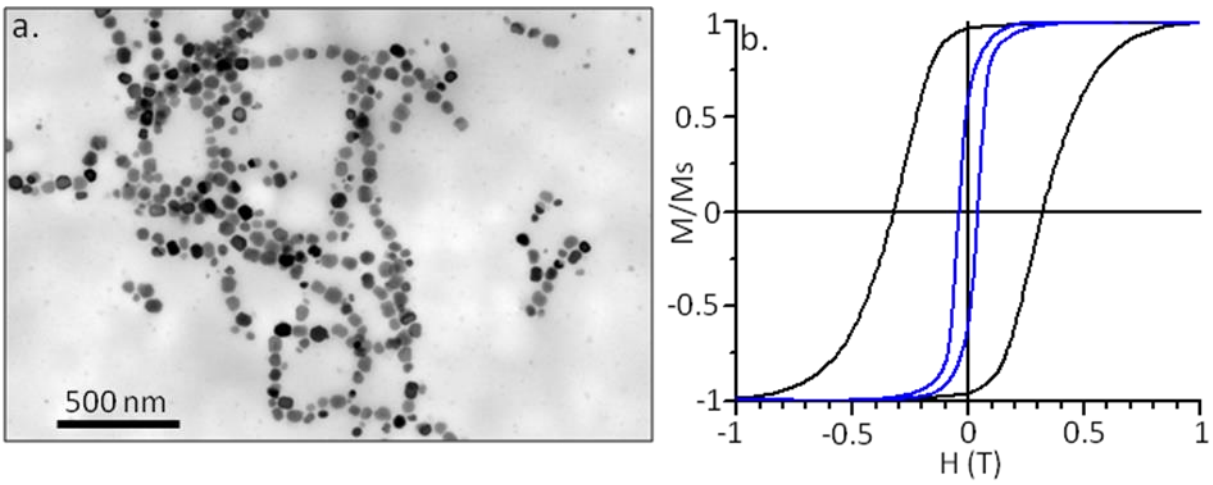

Figure 1

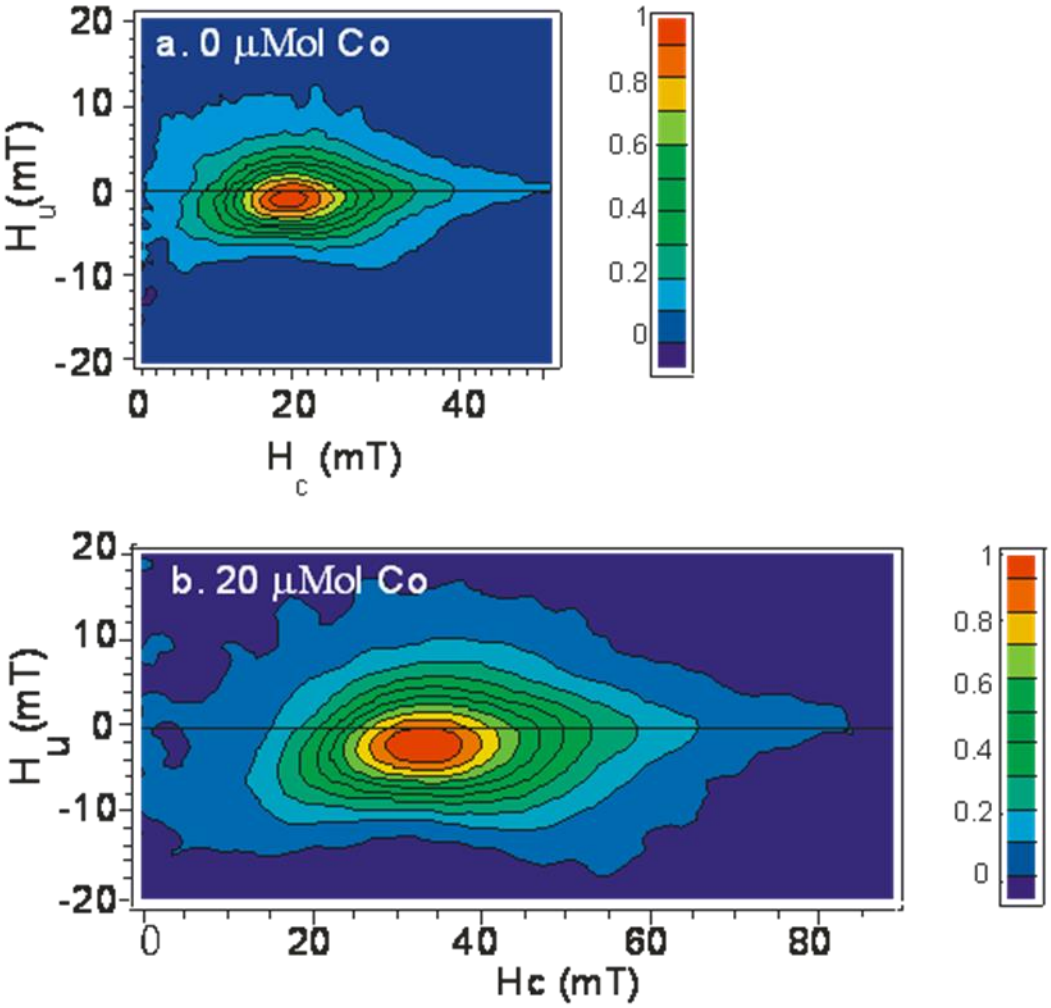
a. 0 μMol Co
20
10
0
-10
-20
H_U (mT)
0
20
40
H_C (mT)
1
0.8
0.6
0.4
0.2
0
b. 20 μMol Co
20
10
0
-10
-20
H_u (mT)
0
20
40
60
80
Hc (mT)
1
0.8
0.6
0.4
0.2
0

Figure 2

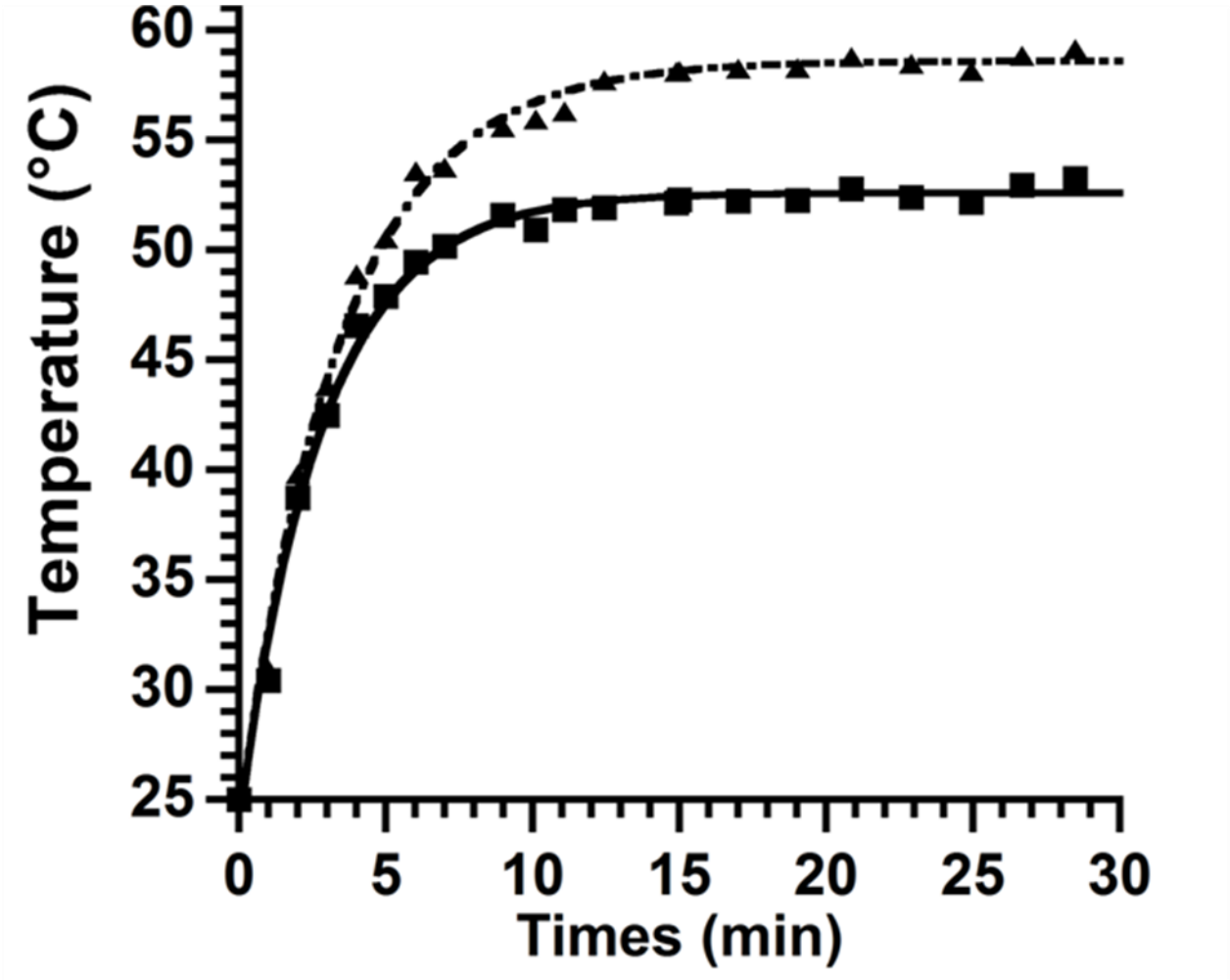

Figure 3

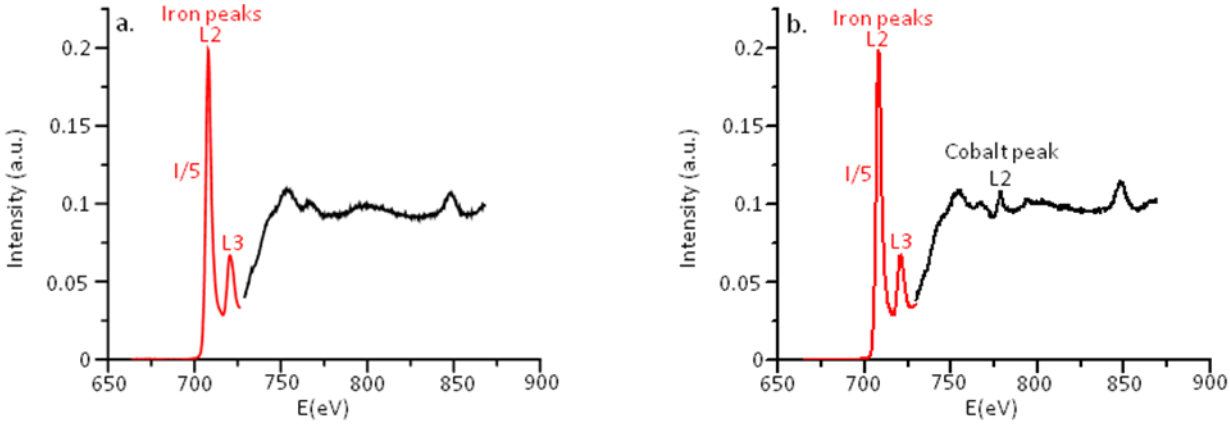
a.
Iron peaks
L2
I/5
L3
Intensity (a.u.)
E(eV)
b.
Iron peaks
L2
Cobalt peak
L2
I/5
L3
Intensity (a.u.)
E(eV)

Suppl. Fig. 1

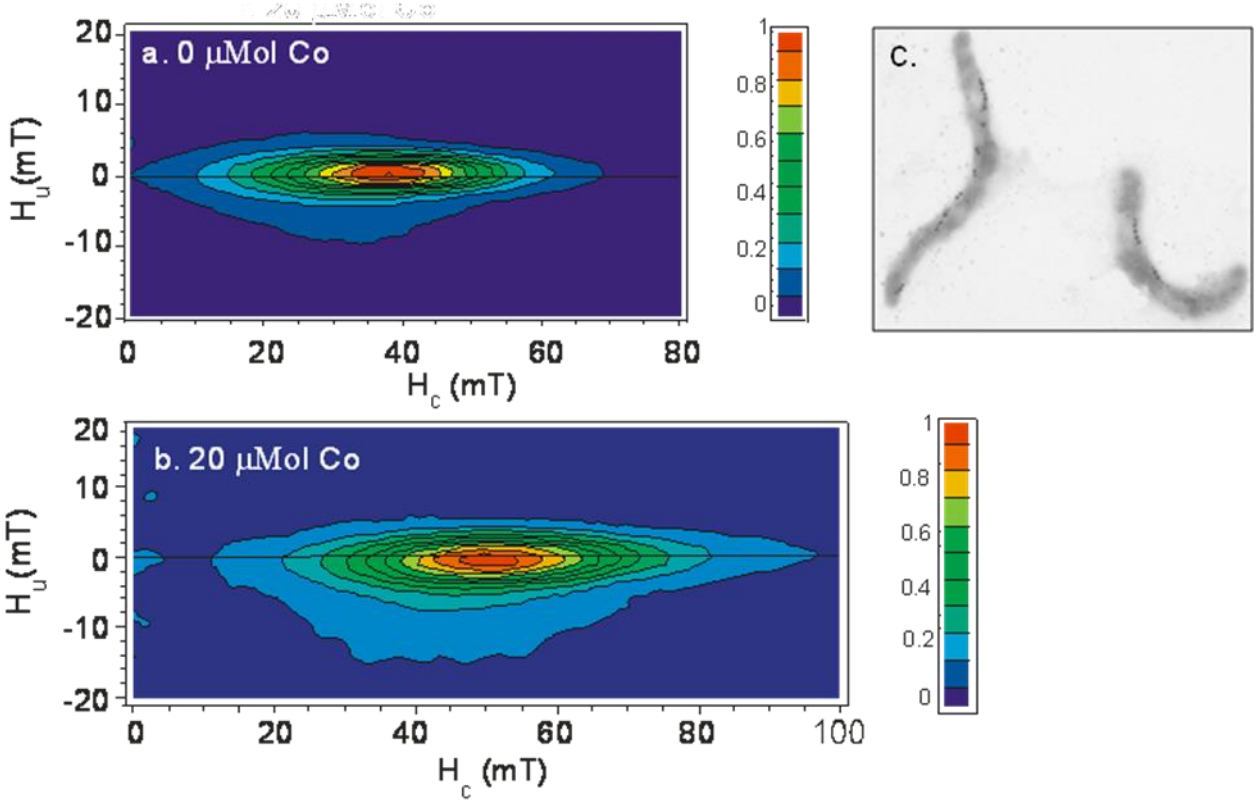
a. 0 μMol Co
b. 20 μMol Co
C.
H_u (mT)
H_c (mT)
20
10
0
-10
-20
0
20
40
60
80
100
1
0.8
0.6
0.4
0.2
0

Suppl. Fig. 2

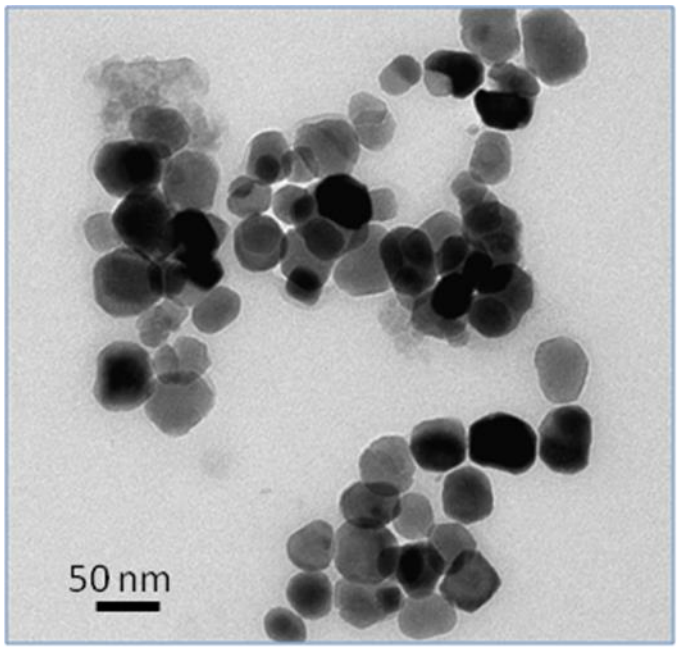

Suppl. Figure 3

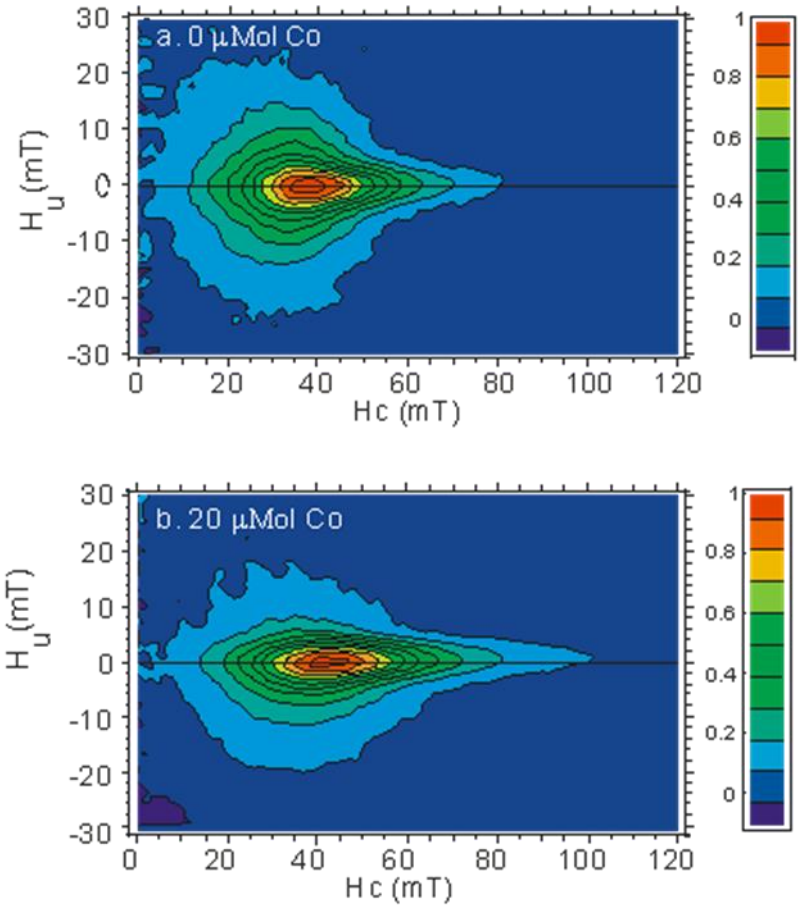

Suppl. Figure 4